08 JST-3662-2022.pdf

WORD COUNT	12021	TIME SUBMITTED	22-MAR-2023 07:19AM
		PAPER ID	97868497

Pertanika J. Sci. & Technol. 31 (2): 781 - 811 (2023)

PERTANIKA JOURNALS

SCIENCE & TECHNOLOGY

Journal homepage: http://www.pertanika.upm.edu.my/

Potential of Fatty Acid Methyl Ester as Diesel Blends Produced from Free Fatty Acid in Waste Cooking Oil Catalyzed by Montmorillonite-Sulfonated Carbon

Hasanudin Hasanudin[1,2]*, Wan Ryan Asri[1,2], Firda Rahmania Putri[1,2], Fahma Riyanti[1,2], Zainal Fanani[1,2], Addy Rachmat[1,2], Novia Novia[3] and Tuty Emilia Agustina[3]

[1]*Department of Chemistry, Faculty of Mathematics and Natural Science, Universitas Sriwijaya, Indralaya 30662, Indonesia*

[2]*Biofuel Research Group, Laboratory of Physical Chemistry, Faculty of Mathematics and Natural Science, Universitas Sriwijaya, Indralaya 30662, Indonesia*

[3]*Department of Chemical Engineering, Department of Engineering, Universitas Sriwijaya, Indralaya 30662, Indonesia*

ABSTRACT

This research, biodiesel production from waste cooking oil (WCO), was conducted using a montmorillonite-sulfonated carbon catalyst from molasses. The biodiesel product would be blended with diesel fuel with various volume variations to see its fuel properties. The catalyst was assessed by Fourier-transform infrared spectroscopy (FTIR), scanning electron microscope (SEM), N_2 adsorption-desorption isotherm, and acidity analysis using the titration method. The effect of the weight ratio of montmorillonite to sulfonated carbon was also evaluated. The process of esterification reaction was optimized using the response surface methodology with a central composite design (RSM-CCD). The study showed that the weight ratio of montmorillonite to sulfonated carbon of 1:3 generated the highest acidity of 9.79 mmol/g with a prominent enhanced surface area and was further employed to optimize the esterification reaction. The optimum condition was obtained at a reaction temperature of 78.12°C, catalyst weight of 2.98 g, and reaction time of 118.27 with an FFA conversion of 74.101%. The optimum condition for the mixture of

ARTICLE INFO

Article history:
Received: 19 May 2022
Accepted: 22 July 2022
Published: 06 March 2023

DOI: https://doi.org/10.47836/pjst.31.2.08

E-mail addresses:
hasanudin@mipa.unsri.ac.id (Hasanudin Hasanudin)
wanryanryan@gmail.com (Wan Ryan Asri)
08031281722023@student.unsri.ac.id (Firda Rahmania Putri)
fatechafj@unsri.ac.id (Fahma Riyanti)
zainalf313@unsri.ac.id (Zainal Fanani)
addy.tea@gmail.com (Addy Rachmat)
novia@ft.unsri.ac.id (Novia Novia)
tuty_agustina@unsri.ac.id (Tuty Emilia Agustina)
*Corresponding author

ISSN: 0128-7680
e-ISSN: 2231-8526

FAME and diesel fuel was achieved at the composition of the B20 blend, which met the FAME standard. The reusability study revealed that the catalyst had adequate stability at three consecutive runs, with a reduced performance was 18.60%. The reduction of FFA conversion was due to the leaching of the catalyst's active site. This study disclosed that the FAME generated from the esterification of FFA on WCO-catalyzed montmorillonite-sulfonated carbon had a promising option as biodiesel blends for increasing the quality of commercial diesel.

Keywords: Biodiesel blends, free fatty acid conversion, montmorillonite, optimization, sulfonated carbon, waste cooking oil

INTRODUCTION

The demand for petroleum is rising in tandem with the economic and population expansion rate. Petroleum reserves are depleted due to increased oil usage in transportation and industry. Renewable and ecologically acceptable alternative energy is required to solve the energy sector's growing issues (Sari et al., 2021; Yuliana et al., 2020). It has known that solar, wind, and bioenergy considerably contribute to the resources of global energy production and pollution reductions. Waste resources, for example, have been employed to make biofuels, which can play an essential part in the energy sector and greatly enhance the world's socioeconomic structure (Jamil et al., 2020). Biodiesel is the potential choice among biofuels due to its low toxicity, biodegradable, carbon-neutral emissions with less sulfur, hydrocarbons, and carbon monoxide content. Biodiesel has the primary prospective to replace conventional diesel as a favorable alternative fuel in diesel engines (Chen et al., 2019).

Various raw materials for biodiesel production have been widely developed due to they are directly related to production costs. Generally, raw materials sourced from non-edible oil are much preferable to vegetable oil (Ali et al., 2018). Non-edible oil such as jatropha or castor oil can be used as raw material for biodiesel production. Even though those materials can produce biodiesel, it does not compete directly with food-grade oil and still requires a large plantation area, so their utilization becomes ineffective (Mazubert et al., 2014). In the recent development of biodiesel feedstocks, the uses of oil wastes have been massively studied due to their numerous advantages (Chen et al., 2021). Waste cooking oil (WCO), palm oil waste, animal fat, and grease, as low-cost raw materials, have been utilized for biodiesel production (Boffito et al., 2013). Currently, a large amount of waste oil is specifically generated by the food processing industry, which, unfortunately, is mostly discharged into municipal sewer systems. This condition contributes to the pollution of various areas and potentially poses a hazard to ecosystems and humans (Soegiantoro et al., 2019). This situation indicates implications for broad opportunities to use WCO as biodiesel feedstock.

WCO has high free fatty acid (FFA) content which can be used as a precursor for biodiesel (Sree et al., 2021). In the study of biodiesel production from WCO, the use of catalysts is critical and dramatically affects the effectiveness and efficiency of biodiesel production. Various types of catalysts have been employed to produce biodiesel from WCO. A homogeneous catalyst such as sulfuric acid has a high FFA conversion capability and exhibits a high biodiesel yield (Ding et al., 2012). Nonetheless, the homogeneous catalyst is corrosive and challenging to separate, generates much water due to purification, and takes up high costs (Suwannasom et al., 2016). The heterogeneous catalyst as a prominent component clearly could resolve those problems as indicated it can be separated and reused, which inherently decreases the cost of production and increases the production efficiency (Zik et al., 2020).

Currently, along with the development of science, the types of catalysts are increasingly diverse in the context of biodiesel production from WCO. The heterogeneous catalyst such as eggshells (Gupta & Rathod, 2018; Kamaronzaman et al., 2020b), bimetallic-CaO derived from eggshells (Mansir et al., 2018), bone-based catalysts (Ali et al., 2018; Suwannasom et al., 2016), sulfonated resin/PVA composite (Zhang et al., 2016), solid acid resins (Boffito et al., 2013), tailored magnetic nano-alumina (Bayat et al., 2018), Fe-montmorillonite K10 (Yahya et al., 2020), Mg/Al hydrotalcite (Ma et al., 2016), and sulfonated carbon (Kumar et al., 2020; Nata et al., 2017), have been extensively used and studied in the biodiesel production from WCO. The use of sulfonated carbon catalysts has attracted interest in biodiesel production because highly active sites result in high catalytic activity in FFA conversion (Bastos et al., 2020).

Interestingly, low-cost carbon sources are abundantly available and can be easily functionalized with sulfonate functional groups. Numerous low-cost precursors derived from biomasses have been employed as carbon precursors (Bastos et al., 2020; Farabi et al., 2019; Lathiya et al., 2018; Ngaosuwan et al., 2016; Niu et al., 2018; Rocha et al., 2019). As waste from sugar factories, Molasse has a good prospective as a source of carbon material because they have a fairly high sugar content (Palmonari et al., 2020). Carbon derived from molasses shows good physical, chemical, and absorptive properties (Kumar et al., 2020).

Hence, the carbonization of molasse potentially generated high carbon content, effectively promoting the functionalization of the sulfonated group. In order to increase the sulfonated carbon catalytic activity, it is necessary to combine with layered or porous supported materials (Munir et al., 2021). It has been reported that clay material such as montmorillonite has Bronsted and Lewis acid, which could promote high conversion and catalytic activity (Hasanudin, Asri, Tampubolon, et al., 2022; Yahya et al., 2020). Therefore, combining montmorillonite with sulfonated carbon derived from molasses potentially exhibits a synergetic effect on the FFA conversion from WCO.

Optimization of FFA conversion from WCO is crucial to getting the desired product along with improving the process feasibility and profitability (Al-Sakkari et al., 2020; Helmi et al., 2020; Sahani et al., 2020; Sharma et al., 2019; Tan et al., 2017; Sree et al., 2021). Furthermore, the simultaneous interaction of each process variable also greatly affects the magnitude of the FFA conversion (Tan et al., 2017). Response surface methodology (RSM) with central composite design (CCD) is a statistical tool that can optimize as well as evaluate the interaction of variables (Singh et al., 2018). The RSM-CCD is highly efficient for demonstrating the second-order model of experimental data and provides adequate estimation (Dhawane et al., 2015; Karmakar & Halder, 2021).

According to the literature review, there are neither studies nor explorations regarding the optimization of FFA conversion from WCO using montmorillonite-sulfonated carbon catalyst by RSM-CCD, as well as the potential of FAME produced as diesel blends. In this study, RSM-CCD was employed to determine the optimum FFA conversion derived from WCO as a response variable using a montmorillonite-sulfonated carbon catalyst. The process variables were assessed: reaction time, catalyst weight, and reaction temperature. The effect of the montmorillonite to sulfonated carbon ratio on the acidity catalyst was evaluated. The catalyst was characterized using FTIR, SEM, and N_2 adsorption-desorption isotherm. The reusability of the catalyst was investigated in three consecutive cycles. Moreover, to see the potential of fatty acid methyl ester (FAME) derived from WCO as diesel blends, the FAME product would be blended with diesel fuel with various volume variations to see its physicochemical properties such as water content, density, volume distillate, kinematic viscosity, and pour point, color, and cetane index.

MATERIALS AND METHODS

Preparation of Catalyst

Briefly, 200-mesh of natural montmorillonite was washed using demineralized water and dried at 120°C for 24 hours in the oven. Next, various weight ratios of montmorillonite to molasses were dissolved in 500 ml of demineralized water, namely 3:1, 2:1, 1:1, 1:2, 1:3, 1:4 (% w/w), and stirred for 1 hour at 80°C. The mixture was later dried in the oven at 120°C. According to Suganuma et al. (2012), the carbonization was conducted with some modifications by employing a temperature of 400°C for 15 hours in the N_2 atmosphere. The powder was referred to as montmorillonite-carbon composites. The sulfonation was conducted using 20 g of the montmorillonite-carbon composite and mixed with 100 ml of concentrated H_2SO_4 in the reflux system at 175°C for 15 hours. After that, the powder was washed with hot water until the pH was close to neutral, followed by centrifugation, and dried for one day at 120°C. The powder was referred to as montmorillonite-sulfonated carbon composite. The acidity of the catalyst was determined using the titration method. The catalyst morphology and its elemental content were assessed using SEM (JEOL), whereas

the functional group catalyst was characterized using FT-IR (Shimadzu). The textural properties were characterized using N_2 adsorption-desorption isotherm (Quantachrome NOVA)

Esterification of FFA from WCO

The esterification was conducted under a reflux system. 25 g of WCO was mixed with 79 ml of methanol, followed by the montmorillonite-sulfonated carbon composite catalyst from molasses. The esterification product was separated from the catalyst. Subsequently, 50 mL of distilled water was added and allowed to stand until two layers, such as FAME and glycerol, were formed. The FAME was later distilled to remove the alcohol and water. The product was characterized using FTIR. The FFA content was analyzed using the titration method with NaOH. The FFA conversion (X) was calculated according to Equation 1:

$$X\ (wt\%)=\frac{F_o-F}{F_o} \quad (1)$$

Where F_o and F are the FFA content of feedstock and the esterification product, respectively.

Experimental Design

This study consisted of 17 run experiments to investigate the optimum interaction and conditions in the conversion of FFA from WCO. The design of the experiment using CCD is shown in Table 1. The quadratic model is shown in Equation 2:

$$Y=\alpha_o+\sum_{i=1}^{n}\alpha_i X_i+\sum_{i=1}^{n}\alpha_{ii}X_i^2+\sum_{i=1}^{n-1}\sum_{j=i+1}^{n}\alpha_{ij}X_i X_i \quad (2)$$

Where Y is the response (FFA conversion), α_o is the constant coefficient, whereas α_i, α_{ii}, and b_{ij} are the coefficients for linear, quadratic, and interaction effects, respectively; X_i and X_j are the process variables (Anguebes-Franseschi et al., 2018). The model's fit was evaluated using analysis of variance (ANOVA).

Table 1
The levels of process variables using CCD

Process variable	Unit	Levels				
		-1.628	-1	0	+1	+1.628
Reaction temperature (A)	°C	63.18	70	80	90	96.82
Catalyst weight (B)	g	0.31	1	2	3	3.68
Reaction time (C)	min	69.55	90	120	150	170.45

Catalyst Reusability

Regarding the catalyst reusability study, the spent catalyst after the esterification reaction was vacuum filtered and washed with alcohol four times. The catalyst was later dried and stored for employment in the next cycle of esterification at optimum conditions.

FAME and Diesel Blend Composition

The FAME produced from the highest FFA conversion was blended with diesel fuel with various compositions (Table 2). The sample was shaken for 10 minutes and then allowed to stand for one hour at room temperature.

Table 2
Blend composition of FAME and diesel fuel

Product	FAME		Diesel fuel	
	%	mL	%	mL
B5	5	20	95	380
B10	10	20	90	360
B15	15	60	85	340
B20	20	80	80	320

FAME Characterization

The FAME, diesel, and blended water content were analyzed according to ASTM D6304 using the Karl Fischer method. The density was analyzed according to ASTM D1298 using a hydrometer. ASTM D86 was used to evaluate the distillation volume of fuel. The kinematic viscosity was determined according to ASTM D445. The color of the fuel was analyzed using ASTM D1500. Furthermore, the standard of ASTM D97 and ASTM D4737 was used to evaluate the fuel's pour point and cetane index, respectively. The FAME product was compared to the European FAME standard (EN 14214:2012). The functional groups of FAME were also assessed using FTIR.

RESULTS AND DISCUSSION

Catalyst Characterization

The montmorillonite-sulfonated carbon catalyst was characterized using FT-IR, SEM, and acidity. Figure 1 shows the FT-IR spectra of the catalyst with a variation ratio of montmorillonite to sulfonated carbon of 1:3, 1:1, and 3:1 (% w/w). The absorption peaks at 1087.05 cm^{-1} and 779.23 cm^{-1} were attributed to the interaction of Si-O-Si

and Si-O-Al bonds from montmorillonite (Munir et al., 2021). The absorption band at 3424.2 cm^{-1} indicated stretching vibrations of the hydroxyl groups. Subsequently, the functional groups of C=C and C-H aromatic were observed at 1628.28 cm^{-1} and 665.26 cm^{-1} due to the carbonization of molasses, which formed a polycyclic aromatic carbon compound, respectively (Flores et al., 2019). All peaks appeared in all catalyst variations. The absorption band at 1082 cm^{-1} corresponded to the -SO_3H functional group due to the sulfonation process (Fadhil et al., 2016), whereas the absorption band at 452 cm^{-1} indicated the C-S-C bond (Fauziyah et al., 2020). Furthermore, Figure 1 shows that the sulfonated group intensity gradually increased as the carbon ratio increased. The more molasses composition, thus the more molasses is converted into carbon. This carbon framework could support the catalyst's active site (Tang et al., 2020). Hence, more SO_3H group was functionalized in the polycyclic aromatic carbon.

The effect of the montmorillonite to sulfonated carbon (% w/w) ratio on the acidity of the catalyst is shown in Figure 2. The acidity increased along with the increase in carbon composition. The highly volatile components of molasses are released during the carbonization process, leaving catalyst support with a high carbon content that provides the functionalization of the -SO_3H active site during the sulfonation process (Endut et al., 2017). As molasses weight composition increased, the carbon formation also increased; consequently, a more sulfonated group was effectively attached to the carbon structure. The highest acidity of the catalyst (9.79 mmol/g) was obtained at the montmorillonite to sulfonated carbon 1:3 ratio. This finding was consistent with the FTIR analysis. The H^+ provided by the heterogeneous acid catalyst, the -SO_3H group, was considered the active site, wherein the acidity was positively correlated to the catalytic activity (Xincheng et al., 2019). The sulfonated groups act as a Bronsted acid which could catalyze the esterification of FFA (Bastos et al., 2020). However, a prolonged high-weight ratio of montmorillonite to sulfonated carbon generated a relatively constant catalyst acidity (9.75 mmol/g) because the sulfonation process had already saturated, whereby the hydroxyl groups present in the carbon framework had been sulfonated and reached a maximum so that the acidity of the catalyst tends to remain constant.

The morphology surfaces of montmorillonite and montmorillonite-carbon sulfonated carbon catalyst is shown in Figure 3. Platy particles consisting of stacks of the layered thin structure were observed in Figure 3a. Alshabanat et al. (2013) reported that the typical montmorillonite structure was irregularly shaped and had many sides. Other studies reported similar findings (Munir et al., 2021). The composite of montmorillonite-sulfonated carbon revealed a significant morphological surface change with porous structure due to carbonization followed by sulfonation (Figure 3a). The carbonization process of molasses into carbon increases the number of cavities and pores. This condition increases the contact area over the sulfonated group, enhances the diffusion of alcohol, and promotes efficient interaction of FFA towards the active site (Fonseca et al., 2020).

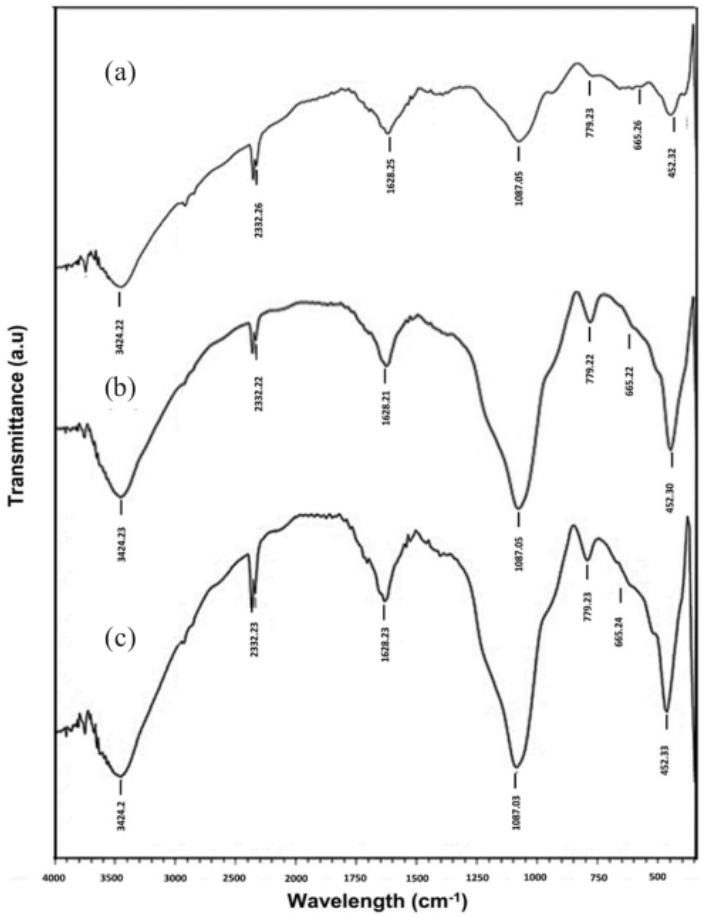

Figure 1. FTIR spectra of montmorillonite-sulfonated carbon of (a) 3:1 (b) 1:1 and (c) 1:3 catalyst

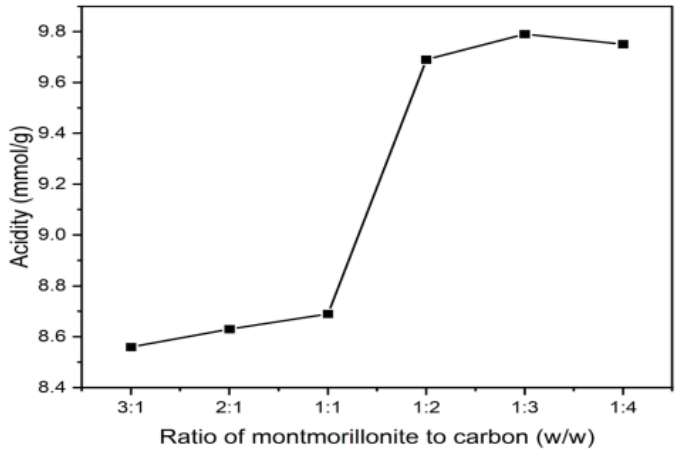

Figure 2. Effect of ratio of montmorillonite to carbon (% w/w) on catalyst acidity

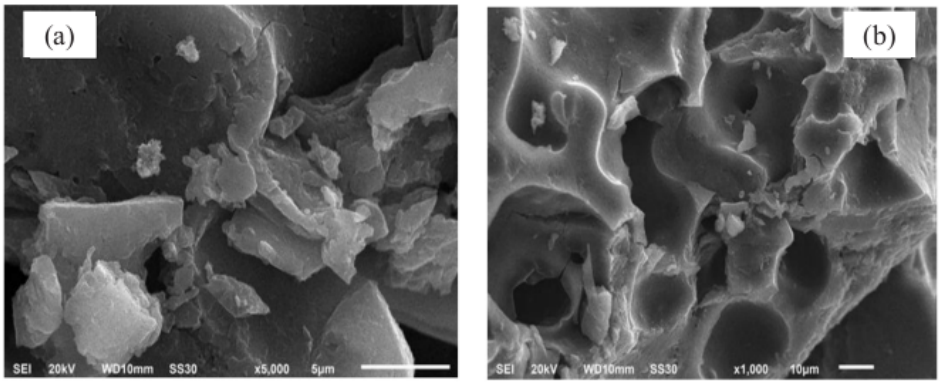

Figure 3. SEM images of (a) montmorillonite and (b) montmorillonite-sulfonated carbon catalyst

Figure 4 shows the N_2 adsorption-desorption of montmorillonite and montmorillonite-sulfonated carbon catalysts. Montmorillonite and montmorillonite-sulfonated carbon revealed type IV isotherm, which had a wide pore distribution (Rabie et al., 2018). Another study reported a similar finding (Lin et al., 2018). It also can be noticed that all catalysts had an H4 hysteresis that corresponded to the aggregates of laminar, which was nearly associated with the layer structure of bentonite (Amaya et al., 2020). Moreover, The typical adsorption-desorption curve at a relative pressure (~0.45) was attributed to the existence of small mesopores on the catalyst (de Oliveira et al., 2019). This small mesopore could promote the high accessibility of the active site. N_2 adsorption-desorption isotherm in Figure 4b revealed a distinctive curve at high relative pressure compared with montmorillonite, and this condition occurred presumably due to the sulfonated carbon effect. This curve was consistent with Lathiya et al. (2018), which utilized the sulfonated carbon catalyst derived from the waste orange peel for esterifying corn acid oil.

Table 3 represents the textural properties of montmorillonite and montmorillonite-sulfonated carbon. The montmorillonite-sulfonated carbon catalyst exhibited high surface area than montmorillonite. The montmorillonite was introduced to the sulfonated carbon, thereby increasing the surface area. A High surface area promoted the extent of the functional group (-SO_3H) to occupy the catalyst surface (Farabi et al., 2019). Furthermore, the increase in surface area was might presumably due to the repulsion force between SO_3H and other groups induced on the catalyst surface (Rahimzadeh et al., 2018).

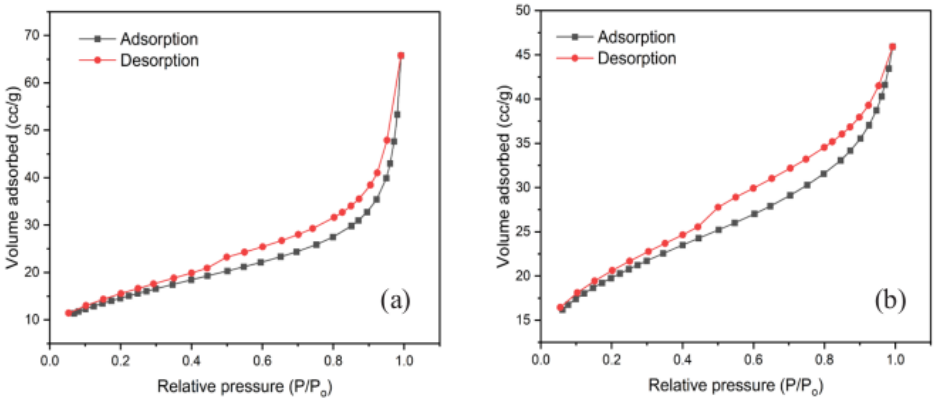

Figure 4. N_2 adsorption-desorption of (a) montmorillonite and (b) montmorillonite-sulfonated carbon catalyst

Table 3

Surface area, total pore volume, and average pore radius of catalysts

Catalyst	Surface area (m^2/g)	Total pore volume (cc/g)	Average pore radius (Å)
Montmorillonite	52.06	0.11	39.09
Montmorillonite-sulfonated carbon	67.12	0.071	21.16

Model Development and ANOVA

In this study, the montmorillonite-sulfonated carbon with a ratio variation of 1:3 was used for optimization because it showed the highest acidity catalyst. The relationship between the response, namely the conversion of FFA, and the process variables, namely reaction temperature, catalyst, and reaction time, were investigated. The experimental design results for 17 runs based on CCD are shown in Table 4. Substantial results were observed in the conversion of FFA under different mild conditions. FFA conversions obtained ranged from 45 to 74.29 %.

Table 4

Experimental result of FFA conversion using CCD

Run	Reaction temperature (˚C)	Catalyst weight (g)	Reaction time (min)	FFA conversion (%)
1	70	1	90	45
2	90	1	90	49.821
3	70	3	90	54.214
4	90	3	90	64.286

Table 4 *(Continue)*

Run	Reaction temperature (°C)	Catalyst weight (g)	Reaction time (min)	FFA conversion (%)
5	70	1	150	47.321
6	90	1	150	56.25
7	70	3	150	73.214
8	90	3	150	74.286
9	63.18	2	120	44.286
10	96.82	2	120	50.179
11	80	0.31	120	47.679
12	80	3.68	120	73.75
13	80	2	69.55	52.679
14	80	2	170.45	55.464
15	80	2	120	65.964
16	80	2	120	65.321
17	80	2	120	65.179

The quadratic model for the conversion of FFA in the coded form is shown in Equation 3:

$$Y = 65.18 + 2.55A + 8.16B + 3.11C - 0.32AB - 0.61AC + 2.53BC - 5.40A^2 - 0.63B^2 - 2.98C^2 \quad (3)$$

The terms A, B, and C represented the single effect regarding the reaction temperature, catalyst, and reaction time, respectively (Equation 3). AB, AC, and BC represented the interaction effect for each variable, whereas the terms A^2, B^2, and C^2 were the quadratic effects. The positive and negative signs correspond to the synergistic and antagonistic effects on the FFA conversion, respectively (Almadani et al., 2018). The ANOVA of the model (95% confidence level) derived from Equation 3 is shown in Table 5.

The P-value of the model was 0.0060, which indicates that the model was statistical significance (Table 5). Likewise, the model's F-value correlated to the FFA conversion was 8.01. This F-value explained that the model was significant, and there was only a 0.60% chance that this high F-value could occur owing to noise (Balajii & Niju, 2021). Subsequently, the terms B, C, and A^2 showed a P-value of <0.05, which indicated that the terms were statistically significant. Furthermore, a sufficient adequate precision value was observed to be more than 4, which was 9.3020. This condition indicated that the model generated an adequate signal and could navigate the quadratic model design (Boey et al., 2013). The statistical diagnostic was conducted to understand the development of the model

(Figure 5). The normal plot (Figure 5a) revealed a straight line that expressed a decent direct agreement between normal probability (%) and externally studentized residuals (Hasanudin, Asri, Said et al., 2022). It appeared that the response transformation was not required and that there were no major problems with the data's normality (Chandane et al., 2020).

The residual plot (Figure 5b) showed that the data were randomly scattered, indicating that the proposed model accurately described the process (Helmi et al., 2020). Figure 5c shows the plot of the predicted value obtained from the quadratic model with respect experimental value. The predicted value based on the model calculation was close to the experimental data, with the coefficient of determination (R^2) value found to be 0.9115. This R^2 value indicated that the prediction model was sufficiently accurate to identify the optimal process parameters with a response variability of 91% (Balajii & Niju, 2021). Figure 5d shows the externally studentized residual respect with a run number plot. The outliers from the run experiments showed that all residual points were in the +3.8 and -3.8 intervals, indicating a good distribution for the CCD design (Noshadi et al., 2012). The leverage respect with a run number plot is shown in Figure 5e. According to the plot, all points are less than one, which was associated with no significant error that could affect the model. Furthermore, the parameter of Cook's distance in Figure 5f revealed that all the points were under the expected, which attributed that there was no significant error in observation (Kusumaningtyas et al., 2021). All statistical diagnostics indicated that the proposed quadratic model was proficient in optimizing the FFA conversion using montmorillonite-sulfonated carbon from a molasses catalyst.

Table 5
ANOVA for the quadratic model

Source	Sum of square	df	Mean	F-value	P-value	
Model	1559.27	9	173.25	8.01	0.0060	significant
A-Reaction temperature	88.70	1	88.70	4.10	0.0825	
B-Catalyst weight	909.58	1	909.58	42.07	0.0003	
C-Reaction time	131.85	1	131.85	6.10	0.0429	
AB	0.8489	1	0.8489	0.0393	0.8486	
AC	2.99	1	2.99	0.1384	0.7209	
BC	51.26	1	51.26	2.37	0.1675	
A^2	328.99	1	328.99	15.22	0.0059	
B^2	4.55	1	4.55	0.2106	0.6602	
C^2	100.39	1	100.39	4.64	0.0681	
Residual	151.34	7	21.62			
Lack of Fit	150.99	5	30.20	172.5821	0.0058	
Pure Error	0.3499	2	0.1750			
Cor Total	1710.61	16				

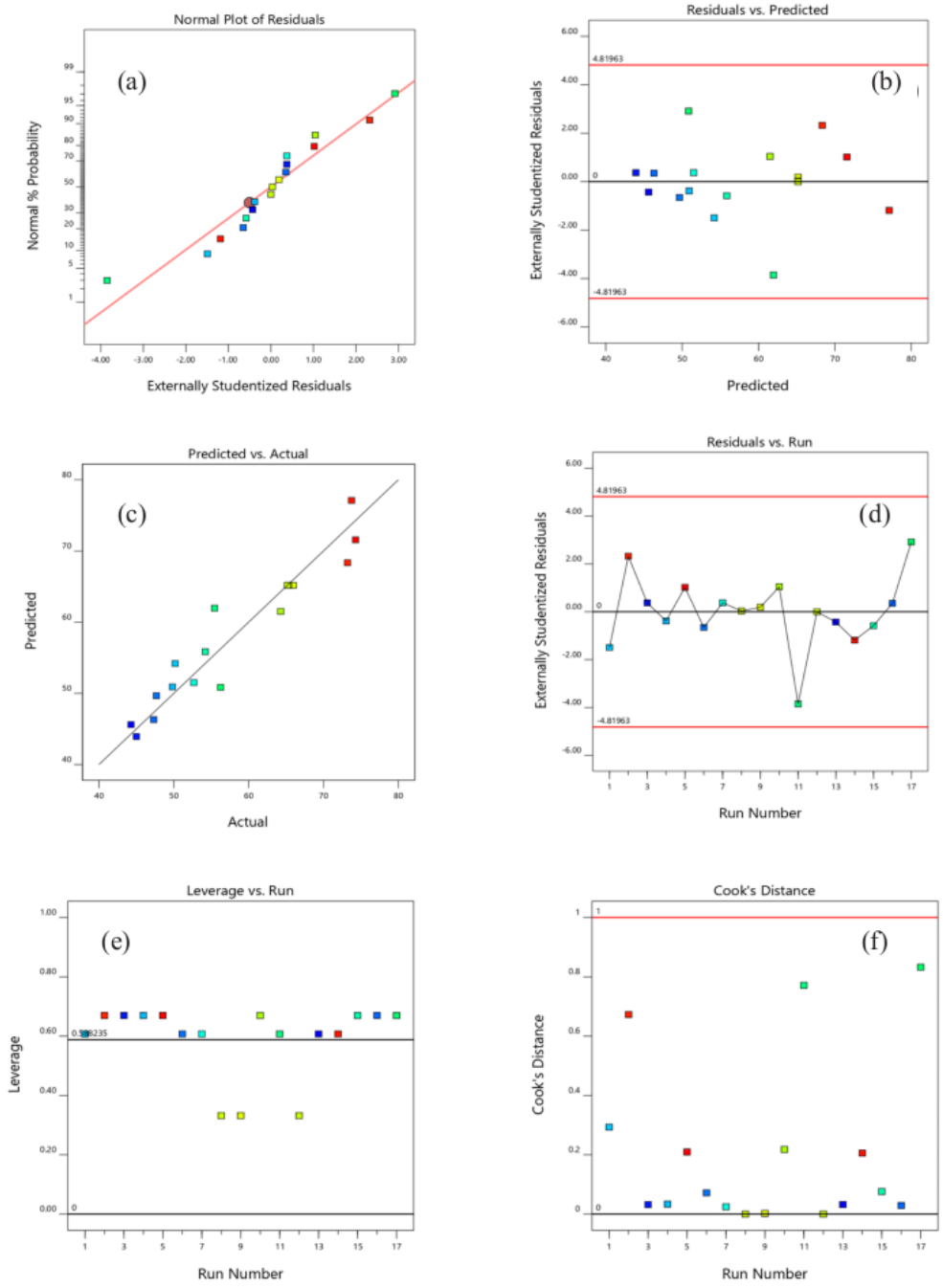

Figure 5. The statistical diagnostic of the development model

Optimization Study

Graphical and numerical optimization procedures were used to predict the optimum conditions of three factors, including reaction temperature, catalyst weight, and reaction time, which resulted in the desired goal of the response variable, namely FFA conversion. The response surface and contour plots were assessed to see the interaction of variables (Figure 6). The interaction effect of a catalyst weight and a reaction temperature at a constant reaction time of 120 min is shown in Figure 6a. The highest FFA conversion was achieved up to 70% when the catalyst weight was higher than 3 g, and the reaction temperature ranged from 70–90°C. Under these conditions, a high catalyst weight presumably increased the number of active catalyst sites, promoting the high FFA conversion (Anguebes-Franseschi et al., 2018). As the temperature increased to 90°C, the collisions between reactants also increased, sufficiently leading to high FFA conversion. Furthermore, these conditions also tended to reduce the mixture's viscosity, thereby increasing diffusion through the pores (Mulay & Rathod, 2021). Gan et al. (2012) reported that the highest conversion of FFA in WCO was achieved up to 60.2% at a temperature of 65°C and a concentration catalyst of 4 wt.% using Amberlyst-15 catalyst. Özbay et al. (2008) used a series of ion-exchange resins, such as an Amberlyst-based catalyst. They showed that the FFA conversion was achieved up to 45.7% when the temperature was 60°C with 2% wt catalyst concentration. Sulfonated nanomagnetic biochar derived from oil palm empty fruit bunch was employed by Jenie et al. (2020), which revealed that at 2.5%wt catalyst concentration, the oleic acid conversion was exhibited up to 71.2%. The montmorillonite-sulfonated carbon derived from the molasse catalyst was likely promising in catalyzing the FFA esterification in WCO relative to previously reported catalysts.

The interaction effect of reaction time and catalyst weight at a constant reaction temperature of 80°C is presented in Figure 6b. The FFA conversion increased at a high catalyst loading of more than 2 g and reaction time ranged from 90–20 min. The longer reaction time did not result in a substantial increase in the FFA conversion. The reaction would approach equilibrium; therefore, no additional conversion would be generated. Jenie et al. (2020) stated that the considerable drop in conversion at longer reaction periods could be attributed to by-product generation or deactivation of the catalyst's active sites. Suresh et al. (2017) utilized sulfonated polystyrene (PSS) for esterification of FFA in WCO and reported that at a reaction temperature of 75°C and PSS concentration of 2% w/w, the conversion exhibited up to 80.8 %. Zhang et al. (2015) used sulfonated mesoporous carbon for the esterification of FFA and showed that a prolonged reaction time of up to three hours would produce high FFA conversion than 80%, whereas Dawodu et al. (2014) generated high FFA conversion derived from sludge palm oil at 4 hours reaction when employing sulfonated carbon from glucose with *C. inophyllum* seed cake.

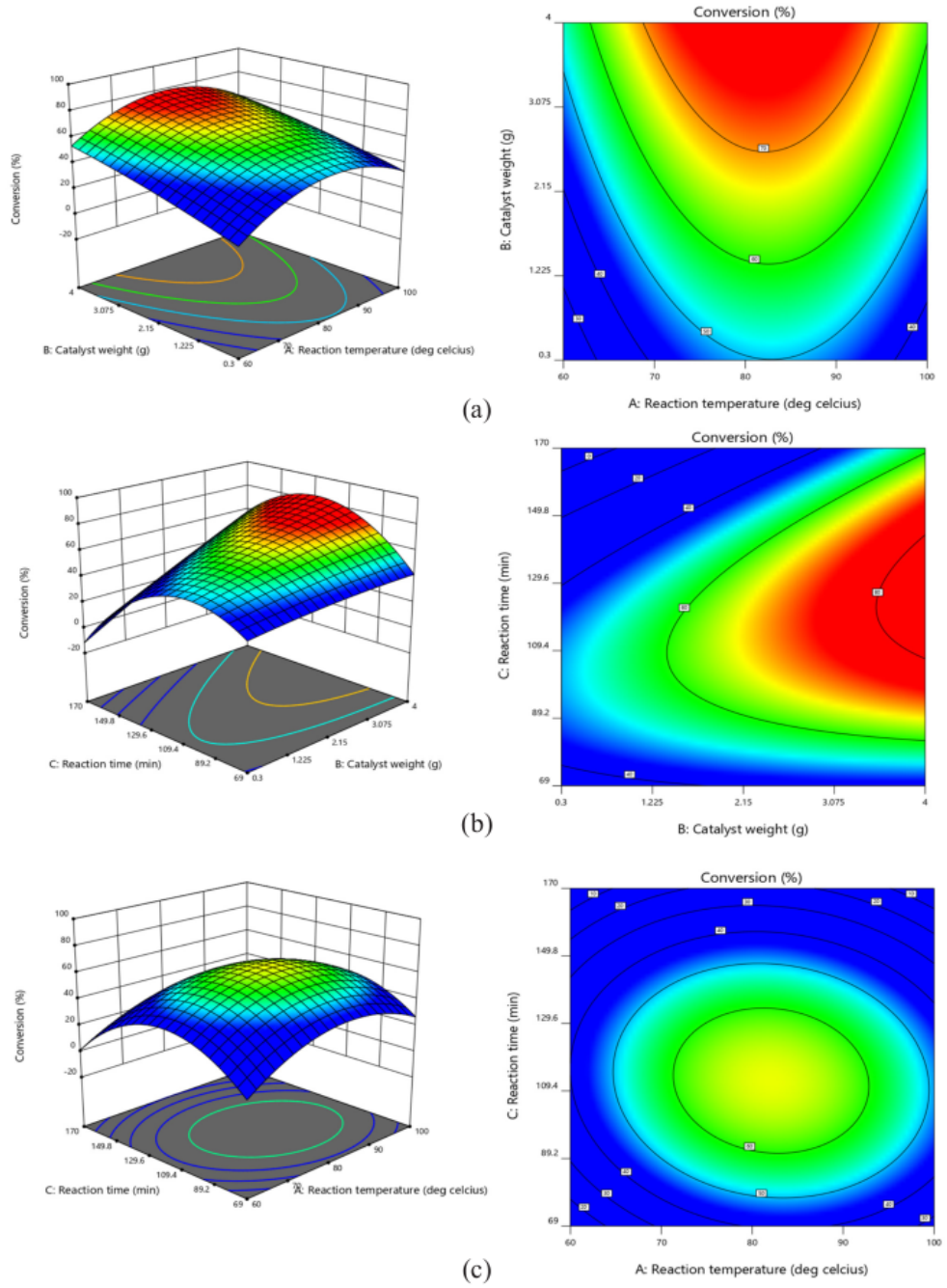

Figure 6. The 3D surface and contour plot of interaction variables on the FFA conversion

The interaction effect of reaction time and reaction temperature at a constant catalyst weight of 2 g is shown in Figure 6c. It was found that the highest FFA conversion was achieved up to 60% at a reaction temperature of 70–90°C and a reaction time of 90–130 min. When the reaction temperature was too high, it would encourage the reverse reaction, decreasing FFA conversion. Simultaneously, the high temperature accelerates the methanol loss rate, potentially reducing catalytic effectiveness (Zhang et al., 2021). As reaction time gradually increased, the FFA conversion also increased due to the availability of sufficient time to complete the reaction (Figure 6c). However, the FFA conversion began to decrease at a long reaction time due to the reverse reaction. These results are also in accordance with the previous report (Narula et al., 2017). Furthermore, a higher reaction time was unfavorable for the esterification reaction since it consumes more energy (Fawaz et al., 2020).

The optimization of FFA conversion by Design-Expert using the numerical method was used to optimize the studied parameters. According to the optimization, the optimum condition was obtained at a reaction temperature of 78.12°C, catalyst weight of 2.98 g, and reaction time of 118.27 with an FFA conversion of 74.101%. In addition, the desirability function was found to be one, which indicated that the developed solution was good. The validation showed that the predicted response was in good accordance with the experimental results.

Catalyst Reusability

The study of catalyst reusability was conducted under the optimized condition obtained from RSM-CCD. Figure 7 represents montmorillonite-sulfonated carbon's reusability performance in FFA conversion at three consecutive runs. It can be noticed that the FFA conversion was slightly decreased in the first cycle. In this first cycle, 70.25% of FFA conversion was achieved, indicating a decrease in the catalyst performance up to 5.07% relative to the fresh catalyst (74% FFA conversion). Moreover, the catalyst's performance was shown significantly reduce up to 9.55% in the second cycle and noticeably decreased in the three consecutive runs, which only generated 60.23% FFA conversion. The decrease in FFA conversion could presumably be due to the active site's leaching, i.e., the sulfonate group (Dhawane et al., 2016). Another study consistently reported a similar finding (Farabi et al., 2019; Tang et al., 2020). This leaching was likely due to insufficient and ineffective regeneration through the alcohol-washing process (Ngaosuwan et al., 2016). In this regard, catalyst regeneration by performing a sulfonation process on the spent catalyst was necessary to return the catalytic activity.

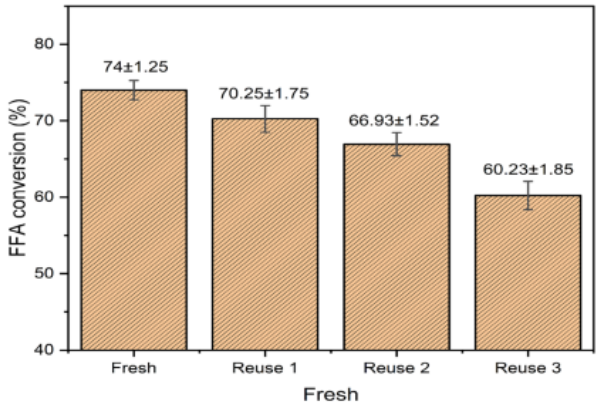

Figure 7. Reusability of catalyst

FAME Physicochemical Properties

The FAME product generated from the optimized esterification reaction and the feedstock, namely WCO, were analyzed using GC and FTIR. GC analysis showed that WCO contained the highest fatty acid composition, namely oleic acid at 43.51% and palmitic acid at 39.75%. This finding was similar to Azman et al. (2021), which reported that WCO consisted of oleic acid (48.1%) as the primary fatty acid, followed by palmitic acid (22%). In contrast, Kumar et al. (2020) found that the WCO consisted of 46.32 wt% palmitic acid and 41.65% oleic acid. These different results are due to the diversity of waste cooking oil sources. The analysis results of FFA content in WCO using the titration method were 36.94%. The FFA content on WCO decreased to 5.938% after esterification using montmorillonite-sulfonated carbon catalyst with a conversion of 83.925%, which indicated that FFA from WCO was potential as a FAME feedstock. In this reaction, the sulfonated groups on the montmorillonite framework act as an active site of Bronsted acid, which could catalyze the esterification of FFA from WCO (Hasanudin, Putri, et al., 2022). The FTIR of WCO and the product of esterification are presented in Figure 8. It can be seen that due to the main structural change was the substitution of methanol in the hydrocarbon chain, the FTIR spectrum of FAME was mainly similar to the WCO, as consistent with previous reports (Kamaronzaman et al., 2020a; Rafati et al., 2019).

The absorption bands from Figure 8a at 2924.02 cm^{-1} and 2854 cm^{-1} were attributed to C-H symmetrical and asymmetrical alkane groups (Banerjee et al., 2019). Subsequently, absorption bands at 1743.65 cm^{-1} corresponded to the ester groups from triglyceride. Furthermore, the region bands at 1458.16 cm^{-1} and 1373.23 cm^{-1} indicated the C-H bending vibration (Mahesh et al., 2015), also revealed in Figure 8b. FAME provided a strong absorption band due to the vibrations of the C=O and C-O bonds. The absorption band at

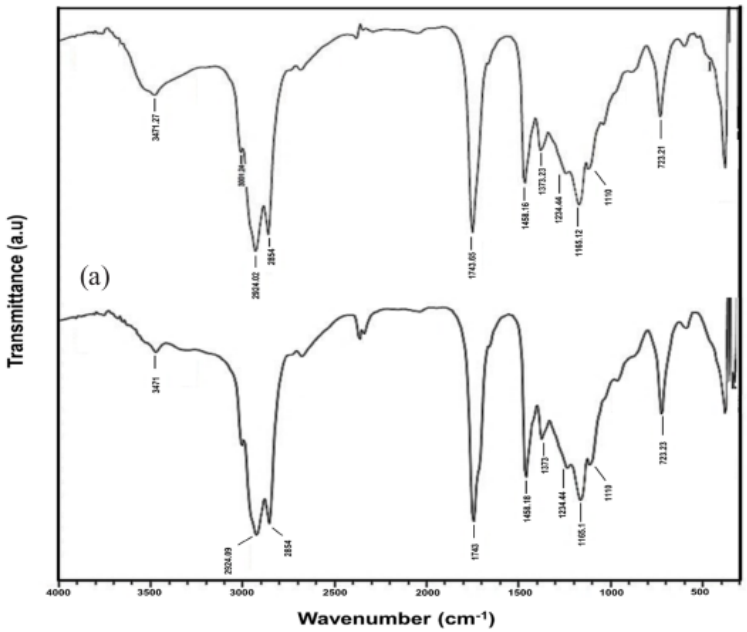

Figure 8. FTIR spectra of (a) WCO and (b) Esterification product

1743.65 cm^{-1} was commonly from the C=O carbonyl group in saturated aliphatic esters (Helmi et al., 2020). The aryl and α,β-unsaturated structures could generate a minor shift in these bands to lower wavenumber (Omidvarborna et al., 2016).

Subsequently, the C-O stretching vibrations appeared at a broader range at 1110 cm^{-1} and were also observed in the FAME spectrum. Long-chain fatty acids in FAME often exhibited an increment to maximum absorption approximately at the absorption band at 1234.44 cm^{-1}, 1165 cm^{-1}, and 723.23 cm^{-1}, respectively (Bahú et al., 2017; Wu et al., 2015). The absorption band at 3471 cm^{-1} indicated the hydroxyl group vibration absorbed by the catalyst (Akram et al., 2019).

The results of the FAME properties analysis from WCO and its standard are shown in Table 6. It shows that the FAME from WCO had a water content of 344 ppm, presumably appearing from palm oil's endocarp component. Besides that, the WCO had been in contact with other components during frying, which caused water's presence. Viscosity and density are the main factors for diesel fuel injection and efficient combustion (Ibeto et al., 2012). The higher the water content in the FAME, led the density (0.8711 Kg/L) and viscosity (4.872 cSt) were also higher. A heavy fraction in the methyl ester accompanies a higher distillation temperature and less distillate (92 mL) that is directly related to the relatively high carbon residue. This condition might inhibit the performance of the diesel engine. The FAME from WCO had the same color characteristics (1.5) as the pure diesel

fuel, which indicated that the FAME had similar good quality. In addition, the cetane index shows a reasonably good value (53.5) above the minimum standard of biodiesel (51). The higher the cetane index of fuel, the better the quality of the fuel as well as provided lower the delay period in the engines (Abdelhady et al., 2020). These results indicated that the FAME derived from WCO has the potential to be used as a blend to improve the quality of diesel fuel.

Table 6

Physicochemical properties of FAME from WCO

Properties	Units	Results	FAME standard (EN 14214:2012)
Water content	ppm	344	Max. 500
Density	Kg/L	0.8711	0.860-0.900
Volume distillate	mL	92	Min. 90
Kinematic viscosity, 40°C	mm^2/s (cSt)	4.872	3.5-5.0
Pour point	˚C	6	-
Color	-	1.5	-
Cetane index	-	53.5	Min. 51

Effect of the FAME and Diesel Composition Blend

In this study, the FAME product derived from the WCO esterification was blended with diesel with various blends, namely B5, B10, B15, and B20, as previously mentioned. The B0 was referred to as the diesel without adding FAME, whereas the B100 was vice versa. The effect of FAME and diesel composition blend on water content and density are shown in Figure 9.

Analysis of water content using the ASTM D-6304 method showed that the FAME from WCO had a water content of 344 ppm (Figure 9). This value encounters the maximum limit of the biodiesel standard (500 ppm). The water content in methyl esters was quite high since biodiesel's density was close to water; thus, biodiesel was more easily bound to water. When the volume added of FAME to diesel fuel increased, the water content also increased (Figure 9). The lowest water content (314 ppm) was achieved by B5, whereas the highest water content (339 ppm) was achieved by B20. In this study, all blend compositions obtained a water content below 500 ppm, which met the criteria of the biodiesel standard. Most diesel engines are composed of metal, which is corrosive in the combustion chamber. High water content in the fuel could cause the hydrolysis of FAME and provoke the growth of microorganisms, which could block the flow in the combustion engine (Fregolente et al., 2012; Lin & Ma, 2020).

The density of diesel blended increased with the increasing volume of methyl ester added to diesel fuel (Figure 9). FAME contained oleic acid ($C_{18}H_{34}O_2$), almost similar to diesel oil (C_{15}-C_{20}). When the methyl ester of oleic acid was mixed with diesel oil, it increased the length of the bond chain; thereby, the fraction in the blend increased. The density was directly proportional to the molecular weight. Thus, when the molecule's chain length increased, the blend's density also increased (Hajilar & Shafei, 2019). The density of the diesel composition blend ranged from 0.8507 to 0.8615 Kg/L, which indicated that the results follow the density of diesel fuel standards.

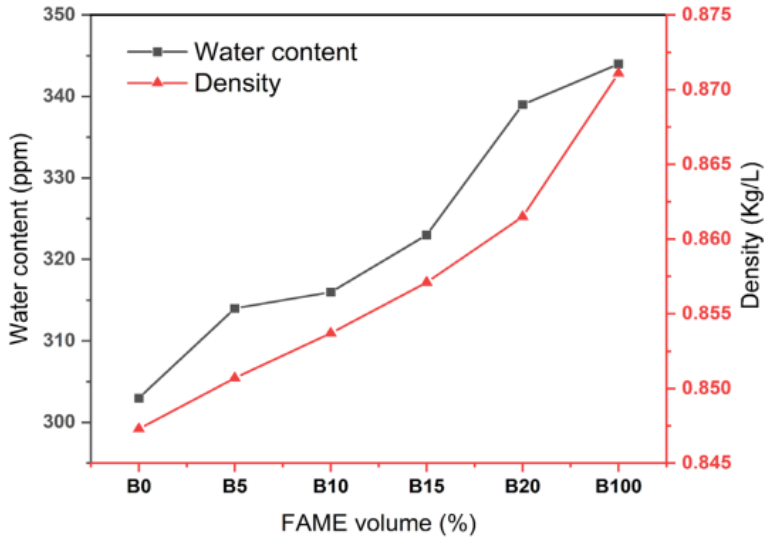

Figure 9. Effect of FAME and diesel composition blend on water content and density

The effect of FAME and diesel composition blend on distillate volume and viscosity are presented in Figure 10. The volume of distillate from the blend of FAME with diesel was lower than the FAME itself, which indicated that the weight fraction in FAME from WCO was relatively high. Similarly, the distillate volume decreased as the amount of FAME added to the diesel blend increased.

Viscosity reveals the lubricating properties of the fuel. Kinematic viscosity measurements using the ASTM D-445 method are conducted to determine the viscosity of fuel or the amount of internal resistance of a liquid to flow related to the supply of fuel consumption in the diesel engine combustion chamber. Kinematic viscosity was directly proportional to the length of the carbon chain and density. Subsequently, it can be seen from Figure 10 that the viscosity increased along with the increase of FAME volume to the diesel fuel. As viscosity is directly proportional to molecular weight, adding FAME to diesel would increase the carbon length chain, thereby increasing the viscosity. The higher

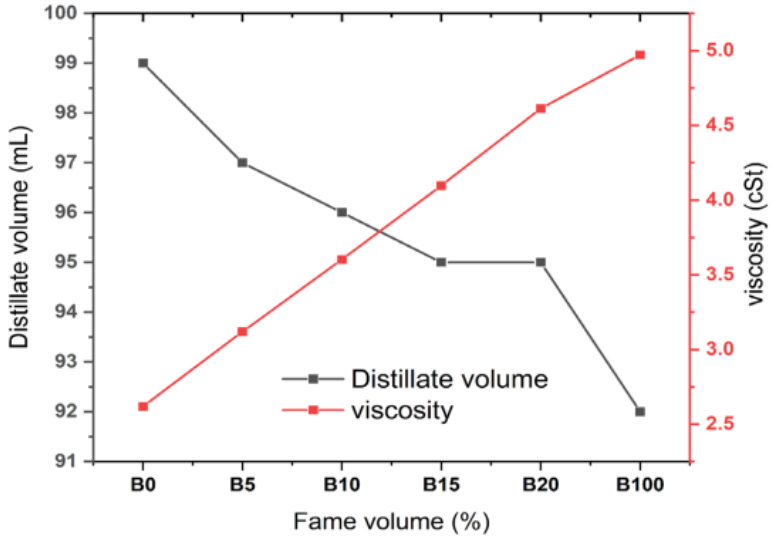

Figure 10. Effect of FAME and diesel composition blend on distillate volume and viscosity

the viscosity, the more difficult the combustion and the slower the piston work. All the blends were in accordance with diesel fuel standards, which corresponded to the engine's good atomization and complete combustion of biodiesel (Karmakar et al., 2018).

Kinematic viscosity measurements using the ASTM D-445 method are conducted to determine the viscosity of fuel or the amount of internal resistance of a liquid to flow related to the supply of fuel consumption in the diesel engine combustion chamber. Kinematic viscosity was directly proportional to the length of the carbon chain and density. Subsequently, it can be seen from Figure 10 that the viscosity increased along with the increase of FAME volume to the diesel fuel. As viscosity is directly proportional to molecular weight, adding FAME to diesel would increase the carbon length chain, thereby increasing the viscosity. The higher the viscosity, the more difficult the combustion and the slower the piston work. All the blends were in accordance with diesel fuel standards, which corresponded to the engine's good atomization and complete combustion of biodiesel (Karmakar et al., 2018).

The effect of FAME and diesel composition blend on color and pour point are shown in Figure 11. Color is a parameter that prevents the possibility of contamination by heavier fuels or water and other substances. This contamination affects the oil quality, resulting in operating failure and engine damage. The color observations results show a linear line on a scale of 1.5 (max. standard diesel = 3), which indicated that the FAME derived from WCO and their blends had a fairly good quality because they had an observation scale that was relatively close to diesel color (Figure 11).

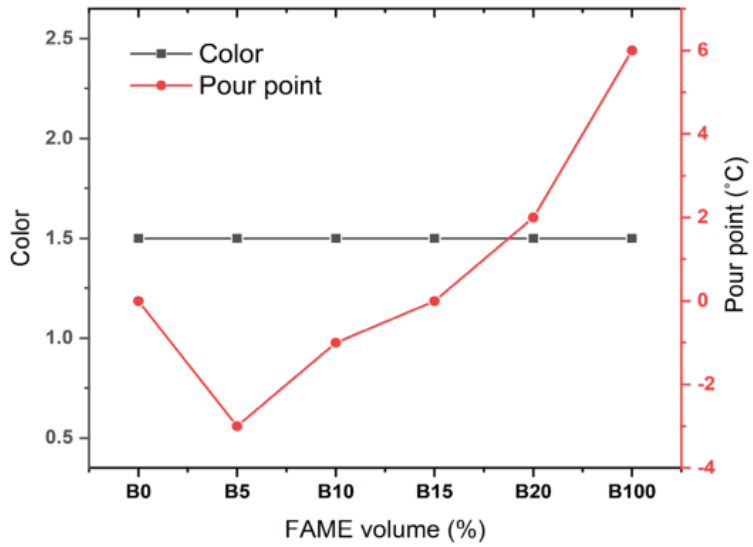

Figure 11. Effect of FAME and diesel composition blend on color and pour point

The pour point of FAME was quite high, at a temperature of 6°C, whereas diesel fuel was achieved at a temperature of 0°C (Figure 11). The pour points of B5 and B10 reached low temperatures of -3°C and -1°C, respectively, exceeding the pour point of pure diesel, whereas, in a blend of B15, the pour point was the same as the pure diesel, which was 0°C. Furthermore, the pour point of the B20 blend increased closer to FAME. The lower the pour point of the fuel, the better the engine's combustion quality because the fuel could still work to lubricate the engine at the lowest temperature. If the fuel is difficult to flow into the combustion chamber, it signifies that converting heat into motion energy by the piston is increasingly difficult. The type of oil and the content or components present in the oil influences the pour point quantity. In addition, the density, viscosity, and solubility of a gas in oil were also influenced.

The cetane index measurement was conducted to determine the ignition quality of diesel fuel. Diesel engines required a cetane number of roughly 50. The fuel cetane number was a volume percentage of cetane and alpha-methyl naphthalene, wherein cetane has better ignition qualities than alpha-methyl naphthalene. The cetane index was needed to prevent engine knocking. The higher the cetane index of diesel fuel, the better the combustion properties (Giakoumis & Sarakatsanis, 2018). The effect of FAME and diesel composition blend on the cetane index is presented in Figure 12.

The index increases along with the amount of FAME added to the diesel blend (Figure 12). The cetane index of pure diesel was 48.5, whereas, after the addition of FAME (B20), the cetane index of the blend increased up to 51.2%. Furthermore, the blend of B10 and

B15 showed no significant difference in cetane index between the two blends. Generally, biodiesel has a higher cetane number than diesel, ranging from 46 to 70. The length of the hydrocarbon chain contained in the FAME caused the cetane number of biodiesel to be higher than diesel (Mishra et al., 2016). The increase of the cetane number from 48.5 to 51.2 would reduce carbon monoxide emissions by 5.27%. In terms of fuel consumption, increasing the cetane number would reduce both fuel engine consumption and engine noise (Rodríguez-Fernández et al., 2019). The results showed that the cetane index of all blends was in accordance with the standard for diesel, with a minimum cetane number of 48. The higher cetane number of biodiesel than diesel leads to better combustion properties of the engine.

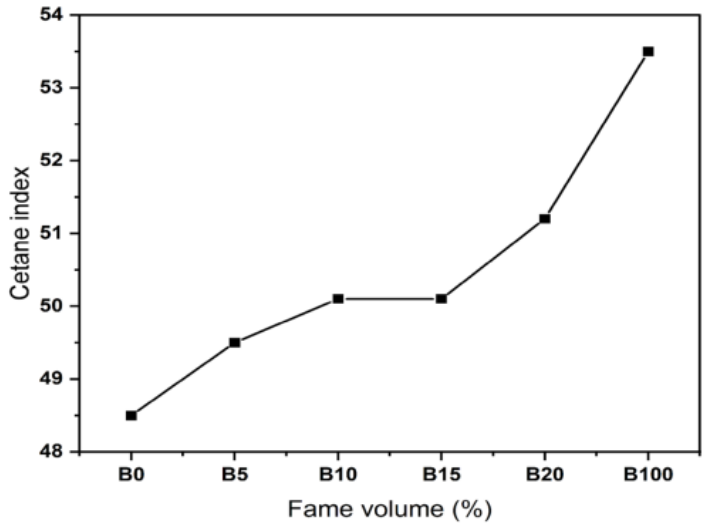

Figure 12. Effect of FAME and diesel composition blend on cetane index

CONCLUSION

In this research, the free fatty acid (FFA) conversion from waste cooking oil (WCO) using montmorillonite-sulfonated carbon catalyst was conducted using response surface methodology (RSM) with a central composite design (CCD). The highest acidity of the catalyst was achieved up to 9.79 mmol/g by montmorillonite to sulfonated carbon 1:3 weight ratio catalyst. The montmorillonite-sulfonated carbon exhibited a higher surface area compared with montmorillonite. The optimum condition was obtained at a reaction temperature of 78.12°C, catalyst weight of 2.98 g, and reaction time of 118.27 with an FFA conversion of 74.101%. A sufficient statistical diagnostic revealed that the RSM-CCD quadratic model could accurately predict the FFA conversion from WCO using a montmorillonite-sulfonated carbon catalyst. The optimum condition for the blend of FAME

and diesel fuel was achieved at the composition of the blend of B20 and in good accordance with the FAME standard. The reusability of the catalyst at three consecutive runs showed that the catalyst had adequate stability but tended to decrease due to the leaching of the active site catalyst.

ACKNOWLEDGEMENTS

The authors thank the Physical Chemistry laboratory and all members of the Biofuel Research Group, Faculty of Mathematics and Natural Science, Universitas Sriwijaya, for supporting research facilities.

REFERENCES

Abdelhady, H. H., Elazab, H. A., Ewais, E. M., Saber, M., & El-Deab, M. S. (2020). Efficient catalytic production of biodiesel using nano-sized sugar beet agro-industrial waste. *Fuel*, *261*, Article 116481. https://doi.org/10.1016/j.fuel.2019.116481

Akram, S., Mumtaz, M. W., Danish, M., Mukhtar, H., Irfan, A., Raza, S. A., Wang, Z., & Arshad, M. (2019). Impact of cerium oxide and cerium composite oxide as nano additives on the gaseous exhaust emission profile of waste cooking oil based biodiesel at full engine load conditions. *Renewable Energy*, *143*, 898-905. https://doi.org/10.1016/j.renene.2019.05.025

Ali, C. H., Asif, A. H., Iqbal, T., Qureshi, A. S., Kazmi, M. A., Yasin, S., Danish, M., & Mu, B. Z. (2018). Improved transesterification of waste cooking oil into biodiesel using calcined goat bone as a catalyst. *Energy Sources, Part A: Recovery, Utilization and Environmental Effects*, *40*(9), 1076-1083. https://doi.org/10.1080/15567036.2018.1469691

Almadani, E. A., Harun, F. W., Radzi, S. M., & Muhamad, S. K. (2018). Cu^{2+} montmorillonite K10 clay catalyst as a green catalyst for production of stearic acid methyl ester: Optimization using response surface methodology (RSM). *Bulletin of Chemical Reaction Engineering & Catalysis*, *13*(1), 187-195. https://doi.org/10.9767/bcrec.13.1.1397.187-195

Al-Sakkari, E. G., Abdeldayem, O. M., El-Sheltawy, S. T., Abadir, M. F., Soliman, A., Rene, E. R., & Ismail, I. (2020). Esterification of high FFA content waste cooking oil through different techniques including the utilization of cement kiln dust as a heterogeneous catalyst: A comparative study. *Fuel*, 279, Article 118519. https://doi.org/10.1016/j.fuel.2020.118519

Alshabanat, M., Al-Arrash, A., & Mekhamer, W. (2013). Polystyrene/montmorillonite nanocomposites: Study of the morphology and effects of sonication time on thermal stability. *Journal of Nanomaterials*, *2013*, Article 650725. https://doi.org/10.1155/2013/650725

Amaya, J., Suarez, N., Moreno, A., Moreno, S., & Molina, R. (2020). Mo or W catalysts promoted with Ni or Co supported on modified bentonite for decane hydroconversion. *New Journal of Chemistry*, *44*(7), 2966-2979. https://doi.org/10.1039/c9nj04878b

Anguebes-Franseschi, F., Abatal, M., Bassam, A., Soberanis, M. A. E., Tzuc, O. M., Bucio-Galindo, L., Quiroz, A. V. C., Ucan, C. A. A., & Ramirez-Elias, M. A. (2018). Esterification optimization of crude African palm olein using response surface methodology and heterogeneous acid catalysis. *Energies*, *11*(1), Article 157. https://doi.org/10.3390/en11010157

Azman, N. S., Marliza, T. S., Asikin-Mijan, N., Hin, T. Y. Y., & Khairuddin, N. (2021). Production of biodiesel from waste cooking oil via deoxygenation using Ni-Mo/Ac catalyst. *Processes*, *9*(5), Article 750. https://doi.org/10.3390/pr9050750

Bahú, J., Hernandez, N., Bonon, A., Bonon, A. D. J., Mart, M., & Gregorio, J. (2017). Epoxy monomers obtained from castor oil using a toxicity-free catalytic system Related papers. *Journal of Molecular Catalysis A: Chemical*, *426*, 550-556.

Balajii, M., & Niju, S. (2021). Esterification optimization of underutilized Ceiba pentandra oil using response surface methodology. *Biofuels*, *12*(5), 495-502. https://doi.org/10.1080/17597269.2018.1496384

Banerjee, S., Sahani, S., & Sharma, Y. C. (2019). Process dynamic investigations and emission analyses of biodiesel produced using Sr-Ce mixed metal oxide heterogeneous catalyst. *Journal of Environmental Management*, *248*, Article 109218. https://doi.org/10.1016/j.jenvman.2019.06.119

Bastos, R. R. C., da Luz Corrêa, A. P., da Luz, P. T. S., da Rocha Filho, G. N., Zamian, J. R., & da Conceição, L. R. V. (2020). Optimization of biodiesel production using sulfonated carbon-based catalyst from an amazon agro-industrial waste. *Energy Conversion and Management*, *205*, Article 112457. https://doi.org/10.1016/j.enconman.2019.112457

Bayat, A., Baghdadi, M., & Bidhendi, G. N. (2018). Tailored magnetic nano-alumina as an efficient catalyst for transesterification of waste cooking oil: Optimization of biodiesel production using response surface methodology. *Energy Conversion and Management*, *177*, 395-405. https://doi.org/10.1016/j.enconman.2018.09.086

Boey, P. L., Ganesan, S., Maniam, G. P., Khairuddean, M., & Efendi, J. (2013). A new heterogeneous acid catalyst for esterification: Optimization using response surface methodology. *Energy Conversion and Management*, *65*, 392-396. https://doi.org/10.1016/j.enconman.2012.08.002

Boffito, D. C., Pirola, C., Galli, F., Di Michele, A., & Bianchi, C. L. (2013). Free fatty acids esterification of waste cooking oil and its mixtures with rapeseed oil and diesel. *Fuel*, *108*, 612-619. https://doi.org/10.1016/j.fuel.2012.10.069

Chandane, V. S., Rathod, A. P., Wasewar, K. L., & Jadhav, P. G. (2020). Response surface methodology and artificial neural networks for optimization of catalytic esterification of lactic acid. *Chemical Engineering and Technology*, *43*(11), 2315-2324. https://doi.org/10.1002/ceat.202000041

Chen, C., Chitose, A., Kusadokoro, M., Nie, H., Xu, W., Yang, F., & Yang, S. (2021). Sustainability and challenges in biodiesel production from waste cooking oil: An advanced bibliometric analysis. *Energy Reports*, *7*, 4022-4034. https://doi.org/10.1016/j.egyr.2021.06.084

Chen, S. Y., Attanatho, L., Chang, A., Laosombut, T., Nishi, M., Mochizuki, T., Takagi, H., Yang, C. M., Abe, Y., Toba, M., Chollacoop, N., & Yoshimura, Y. (2019). Profiling and catalytic upgrading of commercial palm oil-derived biodiesel fuels for high-blend fuels. *Catalysis Today*, *332*, 122-131. https://doi.org/10.1016/j.cattod.2018.05.039

Dawodu, F. A., Ayodele, O., Xin, J., Zhang, S., & Yan, D. (2014). Effective conversion of non-edible oil with high free fatty acid into biodiesel by sulphonated carbon catalyst. *Applied Energy*, *114*, 819-826.

de Oliveira, A. de N., de Lima, M. A. B., Pires, L. H. de O., da Silva, M. R., da Luz, P. T. S., Angélica, R. S., Filho, G. N. d. R., da Costa, C. E. F., Luque, R., & do Nascimento, L. A. S. (2019). Bentonites modified

with phosphomolybdic heteropolyacid (HPMo) for biowaste to biofuel production. *Materials*, *12*(9), Article 1431. https://doi.org/10.3390/ma12091431

Dhawane, S. H., Kumar, T., & Halder, G. (2015). Central composite design approach towards optimization of flamboyant pods derived steam activated carbon for its use as heterogeneous catalyst in transesterification of *Hevea brasiliensis* oil. *Energy Conversion and Management*, *100*, 277-287. https://doi.org/10.1016/j.enconman.2015.04.083

Dhawane, S. H., Kumar, T., & Halder, G. (2016). Biodiesel synthesis from *Hevea brasiliensis* oil employing carbon supported heterogeneous catalyst: Optimization by Taguchi method. *Renewable Energy*, *89*, 506-514. https://doi.org/10.1016/j.renene.2015.12.027

Ding, J., Xia, Z., & Lu, J. (2012). Esterification and deacidification of a waste cooking oil (TAN 68.81 mg KOH/g) for biodiesel production. *Energies*, *5*(8), 2683-2691. https://doi.org/10.3390/en5082683

Endut, A., Abdullah, S. H. Y. S., Hanapi, N. H. M., Hamid, S. H. A., Lananan, F., Kamarudin, M. K. A., Umar, R., Juahir, H., & Khatoon, H. (2017). Optimization of biodiesel production by solid acid catalyst derived from coconut shell via response surface methodology. *International Biodeterioration and Biodegradation*, *124*, 250-257. https://doi.org/10.1016/j.ibiod.2017.06.008

Fadhil, A. B., Aziz, A. M., & Al-Tamer, M. H. (2016). Biodiesel production from *Silybum marianum* L. seed oil with high FFA content using sulfonated carbon catalyst for esterification and base catalyst for transesterification. *Energy Conversion and Management*, *108*, 255-265. https://doi.org/10.1016/j.enconman.2015.11.013

Farabi, M. S. A., Ibrahim, M. L., Rashid, U., & Taufiq-Yap, Y. H. (2019). Esterification of palm fatty acid distillate using sulfonated carbon-based catalyst derived from palm kernel shell and bamboo. *Energy Conversion and Management*, *181*, 562-570. https://doi.org/10.1016/j.enconman.2018.12.033

Fauziyah, M., Widiyastuti, W., & Setyawan, H. (2020). Sulfonated carbon aerogel derived from coir fiber as high performance solid acid catalyst for esterification. *Advanced Powder Technology*, *31*(4), 1412-1419. https://doi.org/10.1016/j.apt.2020.01.022

Fawaz, E. G., Salam, D. A., & Daou, T. J. (2020). Esterification of linoleic acid using HZSM-5 zeolites with different Si/Al ratios. *Microporous and Mesoporous Materials*, *294*, Article 109855. https://doi.org/10.1016/j.micromeso.2019.109855

Flores, K. P., Omega, J. L. O., Cabatingan, L. K., Go, A. W., Agapay, R. C., & Ju, Y. H. (2019). Simultaneously carbonized and sulfonated sugarcane bagasse as solid acid catalyst for the esterification of oleic acid with methanol. *Renewable Energy*, *130*, 510-523. https://doi.org/10.1016/j.renene.2018.06.093

Fonseca, J. M., Spessato, L., Cazetta, A. L., Bedin, K. C., Melo, S. A. R., Souza, F. L., & Almeida, V. C. (2020). Optimization of sulfonation process for the development of carbon-based catalyst from crambe meal via response surface methodology. *Energy Conversion and Management*, *217*, Article 112975. https://doi.org/10.1016/j.enconman.2020.112975

Fregolente, P. B. L., Fregolente, L. V., & Wolf MacIel, M. R. (2012). Water content in biodiesel, diesel, and biodiesel-diesel blends. *Journal of Chemical and Engineering Data*, *57*(6), 1817-1821. https://doi.org/10.1021/je300279c

Gan, S., Ng, H. K., Chan, P. H., & Leong, F. L. (2012). Heterogeneous free fatty acids esterification in waste cooking oil using ion-exchange resins. *Fuel Processing Technology*, *102*, 67-72. https://doi.org/10.1016/j.fuproc.2012.04.038

Giakoumis, E. G., & Sarakatsanis, C. K. (2018). Estimation of biodiesel cetane number, density, kinematic viscosity and heating values from its fatty acid weight composition. *Fuel*, 222, 574-585. https://doi.org/10.1016/j.fuel.2018.02.187

Gupta, A. R., & Rathod, V. K. (2018). Waste cooking oil and waste chicken eggshells derived solid base catalyst for the biodiesel production: Optimization and kinetics. *Waste Management*, *79*, 169-178. https://doi.org/10.1016/j.wasman.2018.07.022

Hajilar, S., & Shafei, B. (2019). Thermal transport properties at interface of fatty acid esters enhanced with carbon-based nanoadditives. *International Journal of Heat and Mass Transfer*, *145*, Article 118762. https://doi.org/10.1016/j.ijheatmasstransfer.2019.118762

Hasanudin, H., Asri, W. R., Tampubolon, K., Riyant, F., Purwaningrum, W., & Wijaya, K. (2022). Dehydration isopropyl alcohol to diisopropyl ether over molybdenum phosphide pillared bentonite. *Pertanika Journal of Science & Technology*, *30*(2), 1739-1754. https://doi.org/10.47836/pjst.30.2.47

Hasanudin, H., Asri, W. R., Said, M., Hidayati, P. T., Purwaningrum, W., Novia, N., & Wijaya, K. (2022). Hydrocracking optimization of palm oil to bio-gasoline and bio-aviation fuels using molybdenum nitride-bentonite catalyst. *RSC Advances, 12*(26), 16431-16443. https://doi.org/10.1039/D2RA02438A

Hasanudin, H., Putri, Q. U., Agustina, T. E., & Hadiah, F. (2022). Esterification of free fatty acid in palm oil mill effluent using sulfated carbon-zeolite composite catalyst. *Pertanika Journal of Science & Technology*, *30*(1), 377-395. https://doi.org/10.47836/pjst.30.1.21

Helmi, M., Tahvildari, K., Hemmati, A., Aberoomand Azar, P., & Safekordi, A. (2020). Phosphomolybdic acid/graphene oxide as novel green catalyst using for biodiesel production from waste cooking oil via electrolysis method: Optimization using with response surface methodology (RSM). *Fuel, 287*, Article 119528. https://doi.org/10.1016/j.fuel.2020.119528

Ibeto, C. N., Okoye, C. O. B., & Ofoefule, A. U. (2012). Comparative study of the physicochemical characterization of some oils as potential feedstock for biodiesel production. *ISRN Renewable Energy*, *2012*, 1-5. https://doi.org/10.5402/2012/621518

Jamil, U., Khoja, A. H., Liaquat, R., Naqvi, S. R., Omar, W. N. N. W., & Amin, N. A. S. (2020). Copper and calcium-based metal organic framework (MOF) catalyst for biodiesel production from waste cooking oil: A process optimization study. *Energy Conversion and Management*, *215*, Article 112934. https://doi.org/10.1016/j.enconman.2020.112934

Jenie, S. N. A., Kristiani, A., Sudiyarmanto, Khaerudini, D. S., & Takeishi, K. (2020). Sulfonated magnetic nanobiochar as heterogeneous acid catalyst for esterification reaction. *Journal of Environmental Chemical Engineering*, *8*(4), Article 103912. https://doi.org/10.1016/j.jece.2020.103912

Kamaronzaman, M. F. F., Kahar, H., Hassan, N., Hanafi, M. F., & Sapawe, N. (2020a). Analysis of biodiesel product derived from waste cooking oil using fourier transform infrared spectroscopy. *Materials Today: Proceedings*, *31*, 329-332. https://doi.org/10.1016/j.matpr.2020.06.088

Kamaronzaman, M. F. F., Kahar, H., Hassan, N., Hanafi, M. F., & Sapawe, N. (2020b). Optimization of biodiesel production from waste cooking oil using eggshell catalyst. *Materials Today: Proceedings*, *31*, 324-328. https://doi.org/10.1016/j.matpr.2020.06.080

Karmakar, B., & Halder, G. (2021). Accelerated conversion of waste cooking oil into biodiesel by injecting 2-propanol and methanol under superheated conditions: A novel approach. *Energy Conversion and Management*, *247*, Article 114733. https://doi.org/10.1016/j.enconman.2021.114733

Karmakar, R., Kundu, K., & Rajor, A. (2018). Fuel properties and emission characteristics of biodiesel produced from unused algae grown in India. *Petroleum Science*, *15*(2), 385-395. https://doi.org/10.1007/s12182-017-0209-7

Kumar, S., Shamsuddin, M. R., Farabi, M. S. A., Saiman, M. I., Zainal, Z., & Taufiq-Yap, Y. H. (2020). Production of methyl esters from waste cooking oil and chicken fat oil via simultaneous esterification and transesterification using acid catalyst. *Energy Conversion and Management*, *226*, Article 113366. https://doi.org/10.1016/j.enconman.2020.113366

Kusumaningtyas, R. D., Prasetiawan, H., Putri, R. D. A., Triwibowo, B., Kurnita, S. C. F., Anggraeni, N. D., Veny, H., Hamzah, F., & Rodhi, M. N. M. (2021). Optimisation of free fatty acid removal in nyamplung seed oil (*Callophyllum inophyllum* l.) using response surface methodology analysis. *Pertanika Journal of Science and Technology*, *29*(4), 2605-2623. https://doi.org/10.47836/PJST.29.4.20

Lathiya, D. R., Bhatt, D. V., & Maheria, K. C. (2018). Synthesis of sulfonated carbon catalyst from waste orange peel for cost effective biodiesel production. *Bioresource Technology Reports*, *2*, 69-76. https://doi.org/10.1016/j.biteb.2018.04.007

Lin, C. Y., & Ma, L. (2020). Influences of water content in feedstock oil on burning characteristics of fatty acid methyl esters. *Processes*, *8*(9), Article 1130. https://doi.org/10.3390/PR8091130

Lin, J., Jiang, B., & Zhan, Y. (2018). Effect of pre-treatment of bentonite with sodium and calcium ions on phosphate adsorption onto zirconium-modified bentonite. *Journal of Environmental Management*, *217*, 183-195. https://doi.org/10.1016/j.jenvman.2018.03.079

Ma, Y., Wang, Q., Zheng, L., Gao, Z., Wang, Q., & Ma, Y. (2016). Mixed methanol/ethanol on transesterification of waste cooking oil using Mg/Al hydrotalcite catalyst. *Energy*, *107*, 523-531. https://doi.org/10.1016/j.energy.2016.04.066

Mahesh, S. E., Ramanathan, A., Begum, K. M. M. S., & Narayanan, A. (2015). Biodiesel production from waste cooking oil using KBr impregnated CaO as catalyst. *Energy Conversion and Management*, *91*, 442-450. https://doi.org/10.1016/j.enconman.2014.12.031

Mansir, N., Teo, S. H., Rabiu, I., & Taufiq-Yap, Y. H. (2018). Effective biodiesel synthesis from waste cooking oil and biomass residue solid green catalyst. *Chemical Engineering Journal*, *347*, 137-144. https://doi.org/10.1016/j.cej.2018.04.034

Mazubert, A., Aubin, J., Elgue, S., & Poux, M. (2014). Intensification of waste cooking oil transformation by transesterification and esterification reactions in oscillatory baffled and microstructured reactors for biodiesel production. *Green Processing and Synthesis*, *3*(6), 419-429. https://doi.org/10.1515/gps-2014-0057

Mishra, S., Anand, K., & Mehta, P. S. (2016). Predicting the cetane number of biodiesel fuels from their fatty acid methyl ester composition. *Energy and Fuels*, *30*(12), 10425-10434. https://doi.org/10.1021/acs.energyfuels.6b01343

Mulay, A., & Rathod, V. K. (2021). Microwave-assisted heterogeneous esterification of dibutyl maleate: Optimization using response surface methodology. *Chemical Data Collections*, *34*, Article 100740. https://doi.org/10.1016/j.cdc.2021.100740

Munir, M., Ahmad, M., Mubashir, M., Asif, S., Waseem, A., Mukhtar, A., Saqib, S., Munawaroh, H. S. H., Lam, M. K., Shiong Khoo, K., Bokhari, A., & Loke Show, P. (2021). A practical approach for synthesis of biodiesel via non-edible seeds oils using trimetallic based montmorillonite nano-catalyst. *Bioresource Technology*, *328*, Article 124859. https://doi.org/10.1016/j.biortech.2021.124859

Narula, V., Khan, M. F., Negi, A., Kalra, S., Thakur, A., & Jain, S. (2017). Low temperature optimization of biodiesel production from algal oil using CaO and CaO/Al_2O_3 as catalyst by the application of response surface methodology. *Energy*, *140*, 879-884. https://doi.org/10.1016/j.energy.2017.09.028

Nata, I. F., Putra, M. D., Irawan, C., & Lee, C. K. (2017). Catalytic performance of sulfonated carbon-based solid acid catalyst on esterification of waste cooking oil for biodiesel production. *Journal of Environmental Chemical Engineering*, *5*(3), 2171-2175. https://doi.org/10.1016/j.jece.2017.04.029

Ngaosuwan, K., Goodwin, J. G., & Prasertdham, P. (2016). A green sulfonated carbon-based catalyst derived from coffee residue for esterification. *Renewable Energy*, *86*, 262-269. https://doi.org/10.1016/j.renene.2015.08.010

Niu, S., Ning, Y., Lu, C., Han, K., Yu, H., & Zhou, Y. (2018). Esterification of oleic acid to produce biodiesel catalyzed by sulfonated activated carbon from bamboo. *Energy Conversion and Management*, *163*(17923), 59-65. https://doi.org/10.1016/j.enconman.2018.02.055

Noshadi, I., Amin, N. A. S., & Parnas, R. S. (2012). Continuous production of biodiesel from waste cooking oil in a reactive distillation column catalyzed by solid heteropolyacid: Optimization using response surface methodology (RSM). *Fuel*, *94*, 156-164. https://doi.org/10.1016/j.fuel.2011.10.018

Omidvarborna, H., Kumar, A., & Kim, D. (2016). Science of the total environment variation of diesel soot characteristics by different types and blends of biodiesel in a laboratory combustion chamber. *Science of the Total Environment*, *544*, 450-459. https://doi.org/10.1016/j.scitotenv.2015.11.076

Özbay, N., Oktar, N., & Tapan, N. A. (2008). Esterification of free fatty acids in waste cooking oils (WCO): Role of ion-exchange resins. *Fuel*, *87*(10-11), 1789-1798. https://doi.org/10.1016/j.fuel.2007.12.010

Palmonari, A., Cavallini, D., Sniffen, C. J., Fernandes, L., Holder, P., Fagioli, L., Fusaro, I., Biagi, G., Formigoni, A., & Mammi, L. (2020). Short communication: Characterization of molasses chemical composition. *Journal of Dairy Science*, *103*(7), 6244-6249. https://doi.org/10.3168/jds.2019-17644

Rabie, A. M., Mohammed, E. A., & Negm, N. A. (2018). Feasibility of modified bentonite as acidic heterogeneous catalyst in low temperature catalytic cracking process of biofuel production from nonedible vegetable oils. *Journal of Molecular Liquids*, *254*(2018), 260-266. https://doi.org/10.1016/j.molliq.2018.01.110

Rafati, A., Tahvildari, K., & Nozari, M. (2019). Production of biodiesel by electrolysis method from waste cooking oil using heterogeneous MgO-NaOH nano catalyst. *Energy Sources, Part A: Recovery, Utilization and Environmental Effects*, *41*(9), 1062-1074. https://doi.org/10.1080/15567036.2018.1539139

Rahimzadeh, H., Tabatabaei, M., Aghbashlo, M., Panahi, H. K. S., Rashidi, A., Goli, S. A. H., Mostafaei, M., Ardjmand, M., & Nizami, A. S. (2018). Potential of acid-activated bentonite and SO_3H-functionalized MWCNTs for biodiesel production from residual olive oil under biorefinery scheme. *Frontiers in Energy Research*, *6*, 1-10. https://doi.org/10.3389/fenrg.2018.00137

Rocha, P. D., Oliveira, L. S., & Franca, A. S. (2019). Sulfonated activated carbon from corn cobs as heterogeneous catalysts for biodiesel production using microwave-assisted transesterification. *Renewable Energy*, *143*, 1710-1716. https://doi.org/10.1016/j.renene.2019.05.070

Rodríguez-Fernández, J., Hernández, J. J., Calle-Asensio, A., Ramos, Á., & Barba, J. (2019). Selection of blends of diesel fuel and advanced biofuels based on their physical and thermochemical properties. *Energies*, *12*(11), Article 2034. https://doi.org/10.3390/en12112034

Sahani, S., Roy, T., & Sharma, Y. C. (2020). Smart waste management of waste cooking oil for large scale high quality biodiesel production using Sr-Ti mixed metal oxide as solid catalyst: Optimization and E-metrics studies. *Waste Management*, *108*, 189-201. https://doi.org/10.1016/j.wasman.2020.04.036

Sari, E. P., Wijaya, K., Trisunaryanti, W., Syoufian, A., Hasanudin, H., & Saputri, W. D. (2021). The effective combination of zirconia superacid and zirconia-impregnated CaO in biodiesel manufacturing: Utilization of used coconut cooking oil (UCCO). *International Journal of Energy and Environmental Engineering, 13*, 967-978. https://doi.org/10.1007/s40095-021-00439-4

Sharma, A., Kodgire, P., & Kachhwaha, S. S. (2019). Biodiesel production from waste cotton-seed cooking oil using microwave-assisted transesterification: Optimization and kinetic modeling. *Renewable and Sustainable Energy Reviews*, *116*, Article 109394. https://doi.org/10.1016/j.rser.2019.109394

Singh, V., Belova, L., Singh, B., & Sharma, Y. C. (2018). Biodiesel production using a novel heterogeneous catalyst, magnesium zirconate ($Mg_2Zr_5O_{12}$): Process optimization through response surface methodology (RSM). *Energy Conversion and Management*, *174*, 198-207. https://doi.org/10.1016/j.enconman.2018.08.029

Soegiantoro, G. H., Chang, J., Rahmawati, P., Christiani, M. F., & Mufrodi, Z. (2019). Home-made ECO green biodiesel from chicken fat (CIAT) and waste cooking oil (pail). *Energy Procedia*, *158*, 1105-1109. https://doi.org/10.1016/j.egypro.2019.01.267

Sree, J. V., Chowdary, B. A., Kumar, K. S., Anbazhagan, M. P., & Subramanian, S. (2021). Optimization of the biodiesel production from waste cooking oil using homogeneous catalyst and heterogeneous catalysts. *Materials Today: Proceedings*, *46*(10), 4900-4908. https://doi.org/10.1016/j.matpr.2020.10.332

Suganuma, S., Nakajima, K., Kitano, M., & Hayashi, S. (2012). sp^3-linked amorphous carbon with sulfonic acid groups as a heterogeneous acid catalyst. *ChemSusChem*, *5*(9), 1841-1846. https://doi.org/10.1002/cssc.201200010

Suresh, R., Antony, J. V., Vengalil, R., Kochimoolayil, G. E., & Joseph, R. (2017). Esterification of free fatty acids in non-edible oils using partially sulfonated polystyrene for biodiesel feedstock. *Industrial Crops and Products*, *95*, 66-74. https://doi.org/10.1016/j.indcrop.2016.09.060

Suwannasom, P., Tansupo, P., & Ruangviriyachai, C. (2016). A bone-based catalyst for biodiesel production from waste cooking oil. *Energy Sources, Part A: Recovery, Utilization and Environmental Effects*, *38*(21), 3167-3173. https://doi.org/10.1080/15567036.2015.1137998

Tan, Y. H., Abdullah, M. O., Nolasco-Hipolito, C., & Zauzi, N. S. A. (2017). Application of RSM and Taguchi methods for optimizing the transesterification of waste cooking oil catalyzed by solid ostrich and chicken-eggshell derived CaO. *Renewable Energy*, *114*, 437-447. https://doi.org/10.1016/j.renene.2017.07.024

Tang, Z. E., Lim, S., Pang, Y. L., Shuit, S. H., & Ong, H. C. (2020). Utilisation of biomass wastes based activated carbon supported heterogeneous acid catalyst for biodiesel production. *Renewable Energy*, *158*, 91-102. https://doi.org/10.1016/j.renene.2020.05.119

Wu, Z., Li, H., & Tu, D. (2015). Application of fourier transform infrared (FT-IR) spectroscopy combined with chemometrics for analysis of rapeseed oil adulterated with refining and purificating waste cooking oil. *Food Analytical Methods*, *8*(10), 2581-2587. https://doi.org/10.1007/s12161-015-0149-z

Xincheng, T., Niu, S., Zhao, S., Zhang, X., Li, X., Yu, H., Lu, C., & Han, K. (2019). Synthesis of sulfonated catalyst from bituminous coal to catalyze esterification for biodiesel production with promoted mechanism analysis. *Journal of Industrial and Engineering Chemistry*, *77*, 432-440. https://doi.org/10.1016/j.jiec.2019.05.008

Yahya, S., Wahab, S. K. M., & Harun, F. W. (2020). Optimization of biodiesel production from waste cooking oil using Fe-Montmorillonite K10 by response surface methodology. *Renewable Energy*, *157*, 164-172. https://doi.org/10.1016/j.renene.2020.04.149

Yuliana, M., Santoso, S. P., Soetaredjo, F. E., Ismadji, S., Ayucitra, A., Angkawijaya, A. E., Ju, Y. H., & Tran-Nguyen, P. L. (2020). A one-pot synthesis of biodiesel from leather tanning waste using supercritical ethanol: Process optimization. *Biomass and Bioenergy*, *142*, Article 105761. https://doi.org/10.1016/j.biombioe.2020.105761

Zhang, B., Gao, M., Geng, J., Cheng, Y., Wang, X., Wu, C., Wang, Q., Liu, S., & Cheung, S. M. (2021). Catalytic performance and deactivation mechanism of a one-step sulfonated carbon-based solid-acid catalyst in an esterification reaction. *Renewable Energy*, *164*, 824-832. https://doi.org/10.1016/j.renene.2020.09.076

Zhang, H., Gao, J., Zhao, Z., Chen, G. Z., Wu, T., & He, F. (2016). Esterification of fatty acids from waste cooking oil to biodiesel over a sulfonated resin/PVA composite. *Catalysis Science and Technology*, *6*(14), 5590-5598. https://doi.org/10.1039/c5cy02133b

Zhang, M., Sun, A., Meng, Y., Wang, L., Jiang, H., & Li, G. (2015). High activity ordered mesoporous carbon-based solid acid catalyst for the esterification of free fatty acids. *Microporous and Mesoporous Materials*, *204*, 210-217. https://doi.org/10.1016/j.micromeso.2014.11.027

Zik, N. A. F. A., Sulaiman, S., & Jamal, P. (2020). Biodiesel production from waste cooking oil using calcium oxide/nanocrystal cellulose/polyvinyl alcohol catalyst in a packed bed reactor. *Renewable Energy*, *155*, 267-277. https://doi.org/10.1016/j.renene.2020.03.144

08 JST-3662-2022.pdf

ORIGINALITY REPORT

22%
SIMILARITY INDEX

MATCHED SOURCE

1	jopr.mpob.gov.my Internet	123 words — 2%
	★jopr.mpob.gov.my Internet	2%

EXCLUDE QUOTES	OFF	EXCLUDE SOURCES	OFF
EXCLUDE BIBLIOGRAPHY	ON	EXCLUDE MATCHES	OFF